Electromechanically tunable carbon nanofiber photonic crystal

Cite as:
Rehammar, R., Ghavanini, F., Magnusson, R., Kinaret, J., Enoksson, P., Arwin, H., & Campbell, E. (2012). Electromechanically tunable carbon nanofiber photonic crystal. *Nano Letters*, 13(2), 397-401.

Manuscript received: 24/09/2012; Accepted: 31/12/2012; Article published: 03/01/2013

Electromechanically Tunable Carbon Nanofiber Photonic Crystal**

Robert Rehammar,[1,†] FarzanAlavian Ghavanini,[2] Roger Magnusson,[3] Jari M. Kinaret,[1] Peter Enoksson,[2] Hans Arwin,[3] Eleanor E.B. Campbell[4,5,*]

[1]Department of Applied Physics, Chalmers University of Technology, SE-412 96 Göteborg, Sweden.

[2]Department of Microtechnology and Nanoscience, Chalmers University of Technology, SE-41296Göteborg, Sweden.

[3]Department of Physics, Chemistry and Biology, LinköpingUniversity, SE-581 83, Linköping, Sweden.

[4]EaStCHEM, School of Chemistry, Joseph Black Building, University of Edinburgh, West Mains Road, Edinburgh, EH9 3JJ, UK.

[5]Division of Quantum Phases and Devices, Department of Physics, Konkuk University, Seoul 143-701, Korea.

[†]Current address: Bluetest AB, Götaverksgatan 1, SE-417 55Göteborg, Sweden.

[*]Corresponding author; e-mail: Eleanor.Campbell@ed.ac.uk

[**]HA, RM and EEBC acknowledge instrumentation support from the Knut and Alice Wallenberg Foundation. EEBC acknowledges support from the WCU program through KOSEF funded by MEST (R31-2008-000-10057-0), the EPSRC (EP/H006567/1) and the Swedish Foundation for Strategic Research. RR and JK acknowledge support from theSwedish Foundation for Strategic Research and the Swedish Research Council.

Keywords:
carbon nanofiber, nanoelectromechanics, diffraction, ellipsometry, form factor, tunable photonic crystal

Abstract

We demonstrate an electrically tunable 2D photonic crystal array constructed from vertically aligned carbon nanofibers. The nanofibers are actuated by applying a voltage between adjacent carbon nanofiber pairs grown directly on metal electrodes, thus dynamically changing the form factor of the photonic crystal lattice. The change in optical properties is characterised using optical diffraction and ellipsometry. The experimental results are shown to be in agreement with theoretical predictions and provide a proof-of-principle for rapidly switchable photonic crystals operating in the visible that can be fabricated using standard nanolithography techniques combined with plasma CVD growth of the nanofibers.

Main text

Photonic crystals (PCs), slabs with periodic variation in permittivity and/or permeability,are exciting systems showing several interesting phenomena such as negative refractive indices[1] and extreme light confinement.[2, 3] If a practical means could be found for combining the exciting optical properties with a way of dynamically and flexibly tuning these properties it would open up a vast range of potential applications with unprecedented possibilities for controlling light properties on the nanoscale. There have been several suggestions of approaches for making tunable PCs. These involve for example the use of mechanical strain to modify the properties of waveguide materials,[4, 5] the application of thermal strain[6] or the use of thermo-optically or electro-optically modified materials encapsulated in the pores of PC structures.[7, 8]

In this letter we present a system that uses electrostatic actuation to modify the form factor in a 2D PC formed from carbon nanofibers. This provides a rapid means of modifying the PC properties of systems operating in the visible spectral range that can be easily integrated on chips. The change in the optical properties is studied using optical diffraction and ellipsometry and compared with a theoretical model.

Carbon nanofibers (CNF) are relatives to multi-walled carbon nanotubes (MWNT) where the graphitic concentric cylindrical tubes in CNTs are typically replaced by quasi-conically shaped stacked graphitic sheets or by a bamboo-like structure.[9] They are synthesised using plasma-enhanced chemical vapor deposition. In contrast to MWNT, it is possible to grow the CNF to produce stable individual fibers with their long axis aligned perpendicular to the substrate, known as vertically-aligned carbon nanofibers (VACNF).[10] The optical properties of static VACNF arrays have been reported previously.[11-15] In recent work we have shown that ellipsometry is a powerful technique to determine the band structure of such 2D VACNF PC and can be used to identify symmetry directions and lattice parameters.[15] We have also shown that the main features of the diffraction properties of the VACNF PC can be modelled using standard diffraction theory but observed polarization-dependent diffraction intensities required a consideration of the form factor of the VACNF array

and the role of surface plasmons at the PC-substrate interface to be explained.[13] In this letter we combine these two techniques to characterise tunable VACNF PC.

Tunability is achieved by electrostatic actuation of the VACNFs. The actuation of CNF by applying voltages on the order of 10 V, either between adjacent fibers or between a fiber and a gate electrode, has been demonstrated previously for nanoelectromechanical devices such as three-terminal relays,[16, 17] switches[18, 19] or tunable resonators.[20]

Two-dimensional square VACNF-based PC slabs were fabricated with a lattice constant a = 400 nm and VACNF height $H \approx 1.7\mu m$. VACNFs were grown on top of pairs of interdigitised electrodes. Figure 1 shows a scanning electron microscope image of the final device along with a schematic showing the electrode arrangement. In such a device, when a voltage is applied to the electrodes,the VACNFs on adjacent electrodes are attracted towards each other (in the x-direction) due to the electrostatic force while the VACNFs on the same electrode repel each other. The resulting actuation provides a way to electrostatically modify the form factor dynamically and reversibly, due to the restoring spring force.

Under reasonable assumptions,[14] electrostatic actuation yields a bending profile displacement in the x-direction as a function of height above the substrate z, for the VACNFs following the expression

$$x(z) = \gamma\left(Hz^2 - \frac{z^3}{3}\right) \tag{1}$$

where γ is a parameter depending on the applied voltage, the Young's modulus of the VACNFs and their radius via the second moment of inertia.[14] The distance between two adjacent VACNFs in the x-direction is the lattice constant a. When applying a voltage, the average distance increases (decreases) pairwise, and can be written as $\langle a \rangle^{\pm} = a \pm 2\bar{x} = a \pm \gamma H^3/2$, see inset in Fig. 2. This deformation is what provides the tuning of the PC. The meander electrode array has a lattice constant of $2a$ in the x-direction, giving a unit cell with dimensions $2a$ x a and a basis that includes two CNFs. When a voltage is applied and the VACNFs are actuated, the CNFs bend and the form factor describing the unit cell changes. Since the coupling to light depends on both the unit cell and the form factor, the optical properties can be changed by electrostatic actuation. The snap-in voltage is defined as the voltage at which the system becomes unstable and the VACNF tips snap-in and touch. This happens for a voltage such that $\gamma \sim a/H^3$.[21] The parameter γ depends on specific VACNF properties, such as the Young's modulus and CNF diameter, as well as the electrostatic force experienced by the CNF ($\propto V^{\beta}$, where V is the applied voltage and β is expected to have a value of approximately 2) and therefore, since the actual value can vary strongly for individual CNF,[22] it is difficult to predict the exact snap-in voltage of a particular VACNF pair. When snap-in occurs, a large current passes through the VACNF pair in contact. This usually induces irreversible damage that renders the device

unusable. To avoid this situation, we work with voltages that are expected to be well below the snap-in voltage.

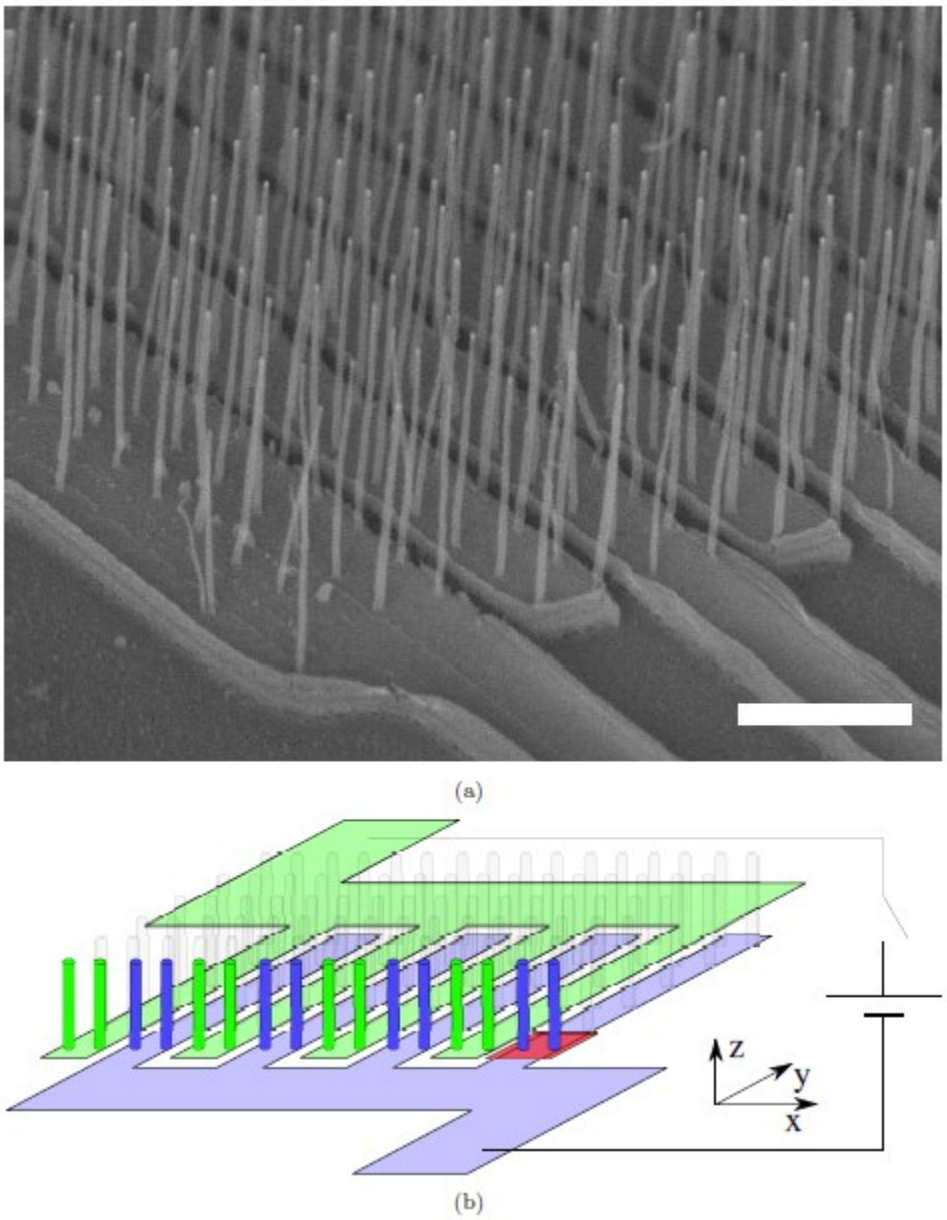

Figure 1. SEM image (a) and pictorial sketch (b) of the system under investigation. The scale bar in (a) is 1 μm. The sketch highlights the two differently biased electrodes by coloring them green and blue. Only the first row of VACNFs are colored, the other rows are only outlined for visibility.

Samples were fabricated from standard silicon wafers with a 400 nm thermally grown oxide layer. TiN electrodes were deposited in a reactive sputtering process and were patterned using electron-beam (e-beam) lithography. The pattern was transferred to the TiN layer in a chlorine-based reactive ion etching (RIE) process.[23] VACNFs were grown from Ni catalyst seeds, 70nm in diameter, which were deposited using e-beam evaporation. The electrodes were patterned in a second e-beam lithography step and the pattern transfer was carried out in a lift-off process.The VACNF growth conditions have been reported in detail earlier.[24] The total PC size was1x1 mm^2, consisting of ~6 million VACNFs.

The diffraction set-up has been described before [13] and consists of a sample holder with translational and rotational degrees of freedom for calibration and selection of incoming and exiting angles of the light beams. A low NA lens, mounted approximately 20 cm away from the sample, couples the light to a fiber which guides the diffracted beam to an Ocean Optics USB 2000 spectrometer, used for the intensity measurements. The modes in the system were excited by a 543.5 nm HeNe laser. Before impinging on the sample, the beam passes through a neutral density filter and a polarizer for controlling light intensity and polarization. Ellipsometric measurements were performed on a dual-rotating-compensator ellipsometer from J. A. Woollam Co., Inc. Incidence angle was $\Theta = 60^o$ from the sample normal.

The type of structure considered here was studied theoretically in an earlier paper. [14] The predicted changes in transmission were related to changes in the band structure of the PC. Here we use reflection spectroscopic ellipsometry with $\pm\Theta$, to mimic in-plane transmission.

The two arrays together create a rectangular lattice with primitive unit cell 2*a*x*a*. The reciprocal lattice vectors are

$$\begin{aligned} \hat{b}_1 &= \left(\frac{2\pi}{a}, 0\right) \\ \hat{b}_2 &= \left(0, \frac{2\pi}{a}\right) \end{aligned} \tag{2}$$

A general reciprocal lattice vector is $\mathbf{G}_{\parallel} = m\hat{b}_1 + n\hat{b}_2$, with *m* and *n* integers. A diffracted light beam is obtained by adding a reciprocal lattice vector to the incoming wavevector.[25] If the incoming beam has a wavevector $\mathbf{k} = \mathbf{k}_{\parallel} + k_z\hat{z}$, a diffracted beam will have the wavevector

$$\mathbf{k'} = \mathbf{k}_{\parallel} + \mathbf{G}_{\parallel} + k_z^{'}\hat{z} \tag{3}$$

where $k_z^{'}$ is determined from energy conservation

$$\mathrm{k'^2} = \mathrm{k^2} \Leftrightarrow k_z^{'2} = k^2 - (\mathbf{k}_{\parallel} + \mathbf{G}_{\parallel})^2. \tag{4}$$

Only diffraction orders where $k_z^{'}$ is real are free-space propagating modes. We number the diffraction orders by the (*m;n*)-tuple.

In our set-up, orders with a combination of *m* = 0;- 1;-2 and *n* = 0;-1 are available. Since periodicity in the *x*-direction comes partially from the electrodes, these take part in the diffraction process for the orders involving $\hat{b}_1$. To be able to separate effects from the electrodes and effects from the VACNF actuation, the order (0,-1), which involves only $\hat{b}_2$, is selected for further investigation in the diffraction set-up.

Results of the diffraction measurements are shown in Fig. 2 where the relative intensity change, δ*I*, for the (0;-1) diffraction order (light propagation in the y-direction) is depicted for *p*- (increasing intensity, blue circles) and *s*-polarization (decreasing intensity, magenta circles). For each voltage *V*, ten repeated pulses were applied and the mean intensity change, δ*I* determined. Each pulse was 2 s long and separated by a 2 s off state (see lower inset). Error bars denote sample standard deviation. As the actuation voltage increases, the fibers become more aligned with the *s*-polarized light and less aligned with the *p*-polarized light. The diffraction intensity increases with applied voltage for *p*-polarization, while it decreases for *s*-polarization. Actuation can be viewed as the VACNFs being tilted by an angle φ around their base, see inset in Figure 2. This changes the alignment of the VACNF. Without an applied voltage, the VACNFs are maximally aligned with *p*-polarized light. With increasing actuation the VACNFs become partially aligned with *s*-polarized light. We have shown previously [13] that the absolute intensity is higher for *s*-polarization than for *p*-polarization in the static case (by approximately 50%) . This was interpreted, and supported by FTDT simulations, as being a consequence of a higher field intensity at the CNFs with *p*-polarized light due to the hybridization of surface plasmon polaritons which are mainly *p*-polarized excitations at the metal electrodes with the surface modes of the CNF lattice.[13] We therefore expect the intensity to increase for *p*-polarization and decrease for *s*-polarization on actuation, as observed. On actuation, the component of *p*-polarized light along the CNF axis is $E_p(\varphi) = E_p(0)\cos\varphi$ and the component of s-polarized light along the CNF axis is $E_s(\varphi) = E_s(0)\sin\varphi$. The change in angle is small and it is only necessary to consider the lowest order in a Taylor expansion of the cos- and sin- terms of the rotation. This then implies that, assuming the losses are proportional to the electric field component along the CNF axis, the loss for *p*-polarized light will be proportional to $-\varphi^2$. In other words, the change in the diffracted intensity is expected to increase with a $\varphi^{2\,2}$ dependence. For *s*-polarized light, the loss will be proportional to φ .and the change in diffracted intensity is expected to decrease linearly with respect to φ. Since $\varphi \approx \gamma H^2/2$ and $\gamma \propto V^{\beta}$, the change in diffracted intensity can be written as $\delta I_{p(s)} = \alpha V^{\beta_{p(s)}}$, with β_p=2β_s. The solid red (dashed green) line in Fig. 2 is a fit $\delta I_{p(s)}(V) = \alpha_{p(s)} V^{\beta p(s)}$ to the *p*(*s*)-data. The resulting

parameters α and β are $(\alpha_p;\beta_p)=(6.2\cdot10^{-6};2\beta_s)$ and $(\alpha_s;\beta_s) = (-2.3\cdot10^{-4};1.6)$. The data clearly show the predicted voltage dependence for the two polarizations.

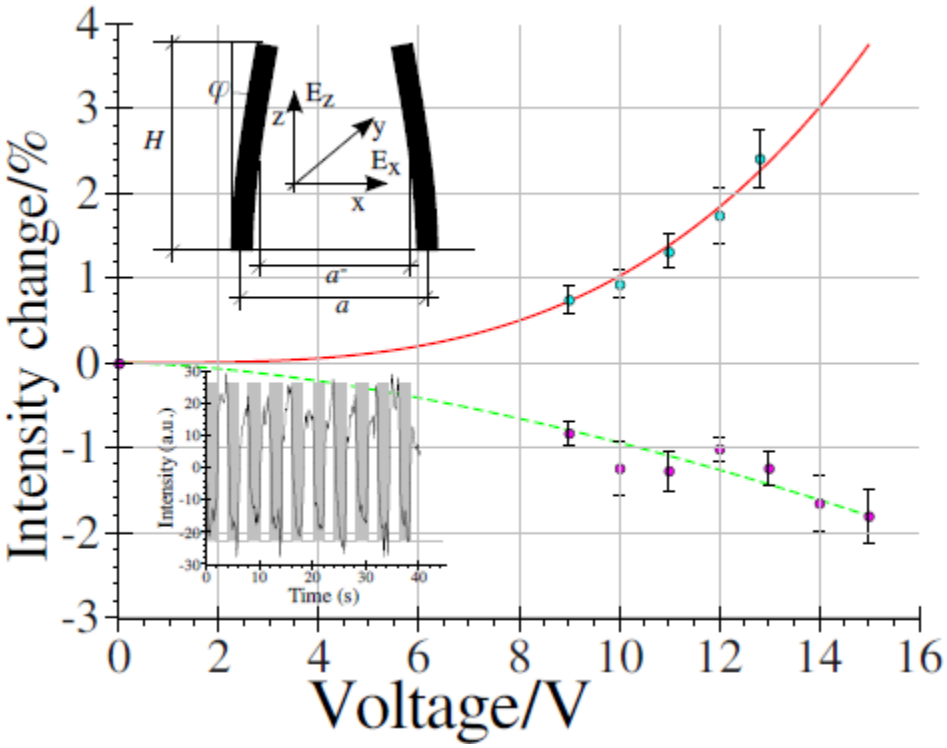

Figure 2. Average relative intensity change in the diffraction measurement, δI as a function of applied voltage, V. The error bars denote the measurement standard deviation. Solid red (dashed green) is a fit to the expression $\delta I=\alpha_{p(s)}(V)^{\beta p(s)}$ for $p(s)$-polarization. Results from ten pulses, each 2 seconds on/off time with an integration time in the spectrometer of approximately 220 ms. The top inset shows the bending profile of two adjacent VACNFs. Also depicted is the electric field vector for each polarization where $E_x=E_s$ and $E_z= E_p\cos\Theta$ where Θ denotes the incidence angle. Bottom inset shows the intensity switching in time for s-polarization after a high pass filter is applied to remove the DC-component of the intensity and any slow drift in the system. Shaded gray area corresponds to when a voltage is applied.

This phenomenologically explains the diffracted intensity variation due to actuation. The exact values of α and β are difficult to obtain theoretically since they depend on many (unknown) properties of the VACNFs and the substrate. It is interesting to note that the tip displacement of the VACNFs is expected to be only a few nm and thus diffraction can detect extremely small displacements, much below the light wavelength.

In an ellipsometric experiment it is not possible to separate the two lattices in a similar manner. We report here the result for actuation in the azimuthal direction of light propagation in the ellipsometer, i.e. the CNF are

actuated in the same direction as the light propagation which, in this case, is the *x*-direction. This makes a comparison to earlier theoretical results more straightforward.[14]

In the ellipsometer data, peaks appear at frequencies corresponding to the Brillouin zone (BZ) edges, see Fig. 3a.[15] Ellipsometry measures the complex reflectance ratio $\rho = R_p / R_s = \tan\Psi e^{i\Delta}$, where R_p and R_s are the amplitudes of the *p*- and *s*-components of the reflected light normalised to their initial values and Ψ and Δ are the ellipsometric angles. Figure 3b shows the change in the ellipsometric angle Ψ [26], for different applied voltages around the peak corresponding to $k_{\|} = k \sin 60^{o} = 7.98\mu m^{-1} \approx 7.85\mu m^{-1} = \pi/a$. This corresponds to the BZ edge of the VACNF square lattice.[15]

The ellipsometry measurements are not as sensitive as the diffraction measurements, yielding only less than 1% change in Ψ at a slightly higher voltage than in the diffraction measurement, Fig. 3. Similar results were obtained for other azimuthal angles (that is, other sample rotations in the plane). It should be pointed out that we did not observe any change in Ψ at frequencies not having an in-plane vector close to a BZ edge. It was also seen in earlier theoretical studies[14], looking at in-plane transmission, that light travelling in the specular direction is not strongly affected by these types of deformations. We associate this with the fact that the static part of the structure (here the substrate) has a strong influence on the optical properties.

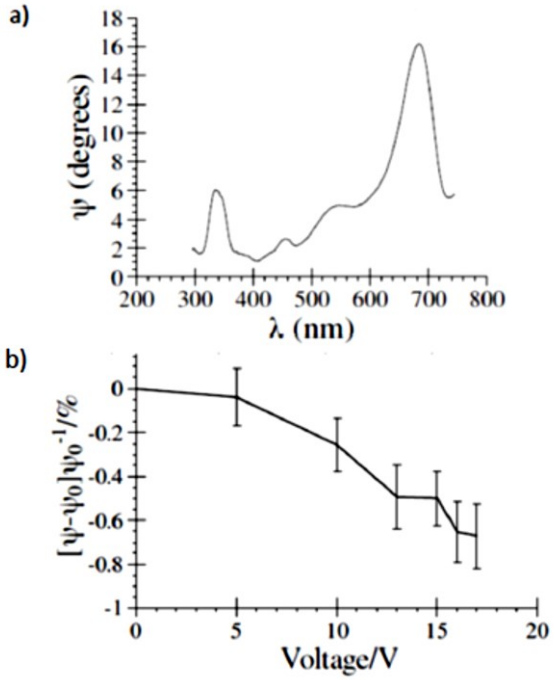

Figure 3. (a) Entire spectrum recorded in the ellipsometer with no applied voltage (b) Relative change, [Ψ(V) - Ψ(0)]/Ψ(0) for the peak centred around 680 nm vacuum wavelength, integrated over frequencies between 667nm and 690 nm. Error bars indicate the measurement standard deviations.

These measurements show that nanowire actuation can be detected optically and also that the light can be modulated by this sub-wavelength actuation. The proof of concept presented here can be exploited by more elaborate designs to realize devices such as on-chip light modulators (including switching and routing) as well as test bench systems for nano-particle plasmonic interaction where the gap between the nano-particles can be dynamically controlled. Moreover,a PC based on VACNFs offers tunability at the nanoscale and therefore can be used to modulate electromagnetic waves at short wavelengths. More elaborate systems can be designed by exploiting the phase shift created through the interaction of incident electromagnetic waves with the actuated VACNFs opening up the opportunity for nanoscale optical phase controlled devices similar to phase controlled antennas found in microwave engineering.

References

[1] A. Berrier, M. Mulot, M. Swillo, M. Qiu, L. Thylén, A. Talneau and S. Anand, Physical Review Letters **93**, 073902 (2004).

[2] M. Loncar, D. Nedeljkovic, T. Doll, J. Vuckovic, A. Scherer and T. P. Pearsall, Applied Physics Letters **77**, 1937 (2000).

[3] B.-S. Song, S. Noda, T. Asano and Y. Akahane, Nature Materials **4**, 207-210 (2005).

[4] S. Rajic, J. L. Corbeil and P. G. Datskos, Ultramicroscopy **97**, 473-479 (2003).

[5] W. Park and J.-B. Lee, Applied Physics Letters **85**, 4845-4847 (2004).

[6] Y. A. Vlasov, M. O'Boyle, H. F. Hamann and S. J. McNab, Nature **438**, 65-69 (2005).

[7] T. Alkeskjold, J. Laegsgaard, A. Bjarklev, D. Hermann, A. Anawati, J. Broeng, J. Li and S.-T. Wu, Optics Express **12**, 5857-5871 (2004).

[8] D.-P. Cai, H.-Y. Pan, J.-F. Tsai, H.-K. Chiu, S.-C. Nian, S. H. Chang, Chen, C.-C. and C.-C. Lee, Optics Materials Express **1** (8), 1471-1477 (2011).

[9] M. S. Kabir, R. E. Morjan, O. Nerushev, P. Lundgren, S. Bengtsson, P. Enoksson and E. E. B. Campbell, Nanotechnology **17**, 790 (2006).

[10] R. E. Morjan, M. S. Kabir, S. W. Lee, O. A. Nerushev, P. Lundgren, S. Bengtsson, Y. W. Park and E. E. B. Campbell, Current Applied Physics **4**, 591-594 (2004).

[11] K. Kempa, B. Kimball, J. Rybczynski, Z. P. Huang, P. F. Wu, D. Steeves, M. Sennett, M. Giersig, D. V. G. L. N. Rao, D. L. Carnahan, D. Z. Wang, J. Y. Lao, W. Z. Li and Z. F. Ren, Nano Letters **3**, 13-18 (2003).

[12] J. Rybczynski, K. Kempa, Y. Wany, Z. F. Ren, J. B. Carlson, B. R. Kimball and G. Benham, Applied Physics Letters **88**, 203122-203123 (2006).

[13] R. Rehammar, Y. Francescato, A. I. Fernandez-Dominguez, S. A. Maier, J. M. Kinaret and E. E. B. Campbell, Optics Letters **37**, 100-102 (2012).

[14] R. Rehammar and J. M. Kinaret, Optics Express **16**, 21682-21691 (2008).

[15] R. Rehammar, R. Magnusson, A. I. Fernandez-Dominguez, H. Arwin, J. M. Kinaret, S. A. Maier and E. E. B. Campbell, Nanotechnology **21**, 465203 (2010).

[16] S. W. Lee, D. S. Lee, R. E. Morjan, S. H. Jhang, M. Sveningsson, O. A. Nerushev, Y. Park, W, and E. E. B. Campbell, Nano Letters **4**, 2027-2030 (2004).

[17] S. Axelsson, E. E. B. Campbell, L. M. Jonsson, J. M. Kinaret, S. W. Lee, Y. W. Park and M. Sveningsson, New Journal of Physics **7**, 245-266 (2005).

[18] J. E. Jang, S. N. Cha, Y. Choi, G. A. J. Amaratunga, D. J. Kang, D. G. Hasko, J. E. Jung and J. M. Kim, Applied Physics Letters **87**, 163114 (2005).

[19] J. E. Jang, S. N. Cha, Y. J. Choi, D. J. Kang, T. P. Butler, D. G. Hasko, J. E. Jung, J. M. Kim and G. A. J. Amaratunga, Nature Nanotechnology **3**, 26-30 (2008).

[20] A. Eriksson, S. W. Lee, A. A. Sourab, A. Isacsson, R. Kaunisto, J. M. Kinaret and E. E. B. Campbell, Nano Letters **8**, 1224-1228 (2008).

[21] G. M. Rebeiz, *RF MEMS*. (John Wiley & Sons, Hoboken, NJ, USA, 2003).

[22] J. G. Lawrence, L. M. Behan and A. Nadarajah, ACS Nano **2**, 1230-1236 (2008).

[23] K. R. Williams, K. Gupta and M. Wasilik, Journal of Nicroelectromechanical Systems **12**, 761-778 (2003).

[24] F. A. Ghavanini, M. Lopez-Damian, D. Rafieian, K. Svensson, P. Lundgren and P. Enoksson, Sensors and Actuators A: Physical **172**, 347-358 (2011).

[25] L. Brillouin, *Propagation in Periodic Structures*. (Dover publications, 1953).

[26] J. Humlicek, in *Handbook of Ellipsometry*, edited by H. G. Tompkins and E. A. Irene (Springer-Verlag GmbH, 2005).